Dynamical vertex approximation: A step beyond dynamical mean-field theory

A. Toschi,[1] A. A. Katanin,[1,2] and K. Held[1]
[1]*Max-Planck-Institut für Festkörperforschung, 70569 Stuttgart, Germany*
[2]*Institute of Metal Physics, 620219 Ekaterinburg, Russia*
(Received 21 September 2006; revised manuscript received 23 November 2006; published 19 January 2007)

We develop a diagrammatic approach with local and nonlocal self-energy diagrams, constructed from the local irreducible vertex. This approach includes the local correlations of dynamical mean-field theory and long-range correlations beyond. It allows us, for example, to describe (para)magnons and weak localization effects—in strongly correlated systems. As a first application, we study the interplay between nonlocal antiferromagnetic correlations and the strong local correlations emerging in the vicinity of a Mott-Hubbard transition.

DOI: 10.1103/PhysRevB.75.045118 PACS number(s): 71.27.+a, 71.10.Fd

I. INTRODUCTION

Strongly correlated electron systems represent both an opportunity and a challenge for modern physics. They are an opportunity because fascinating phenomena occur such as high-temperature superconductivity in cuprates, "colossal" magnetoresistance in manganites, and quantum critical behavior in heavy Fermion compounds. But at the same time they are a challenge because the very same correlations that are responsible for these phenomena make a theoretical understanding and hence an experimental optimization of these effects particularly difficult.

One of the key issues that arises due to strong electronic correlations and that cannot be described by perturbation theory is the Mott-Hubbard metal-insulator transition.[1] In this respect, dynamical mean-field theory (DMFT) (Refs. 2 and 3) was a big step forward to a more thorough understanding of this transition. DMFT becomes exact in the limit of high spatial dimensions ($d \to \infty$) and already accounts for a large (local) part of electronic correlations—the part that provides for the radical changes upon going from a metal to a Mott insulator. Real physical systems are, however, one-, two-, or three-dimensional. Hence, nonlocal correlations, which are neglected in DMFT, may be of importance. Corrections of order $1/d$ have been considered in Ref. 4, resulting in a two-impurity problem, and account for short-range correlations. There has also been recent progress to go beyond DMFT through cluster extensions,[5] which include correlations within the cluster. These correlations are also necessarily short-range in nature due to numerical limitations of the cluster size.[6]

Often, however, long-range correlations are of vital importance. They are responsible for a rich variety of phenomena, ranging from magnons and screening of the Coulomb interaction to quantum criticality. Long-range correlations are also generally pivotal in the vicinity of phase transitions. The existing theories describing long-range (e.g., magnetic) correlations such as the fluctuation exchange approximation,[7] the two-particle self-consistent approximation,[8] and the functional renormalization group[9] are restricted to the weak-coupling regime. For strongly correlated systems, e.g., in the vicinity of a Mott-Hubbard transition, an extension of DMFT by nonlocal (particularly long-range) correlations is therefore needed.

For *static* mean-field theories, such corrections have been studied since decades, e.g., for localized[10] and itinerant magnets;[11,12] for disordered systems, such nonlocal effects have also been considered.[13] But there have been only a very few attempts so far to include long-range correlations beyond dynamical mean-field theory: The DMFT self-energy was supplemented by an "external" **k**-dependent self-energy that describes spin fluctuations in the spin-fermion model[14] or that stems from the self-consistent renormalization theory,[15] and one might also subsume the GW+DMFT approach[16] here. Let us also note the extended DMFT [EDMFT (Ref. 17)], which considers the effect of *nonlocal* interactions on the purely *local* self-energy.

In this paper, we aim at a systematic diagrammatic extension of DMFT by long-range correlations and at an investigation of their effect on the *nonlocal* self-energy. Diagrammatically, DMFT corresponds to all topologically distinct but *local* Feynman diagrams for the self-energy. On the next level, we assume the locality of the fully irreducible two-particle vertex, and consider all (local or nonlocal) self-energy diagrams that can be constructed from this vertex. One might generalize this approach, requiring locality of the fully irreducible n-particle vertex. Then, one has DMFT for $n=1$, the dynamical vertex approximation (DΓA) for $n=2$, and the exact solution for $n \to \infty$. We think, however, that the one- and two-particle levels ($n=1,2$) are the most relevant approximations. If one is interested in a specific physical problem, a restriction of DΓA to certain ladder diagrams is reasonable. In the particle-hole channels, the ladder diagrams yield (para)magnons[11] and random-phase approximation (RPA) screening; in the particle-particle channel, the cooperon diagrams are responsible for attractive pairing interactions and weak localization effects. DΓA includes such ladder diagrams beyond DMFT, but with the local vertex instead of the bare interaction so that strong correlations are accounted for.

In this paper, we introduce DΓA and apply it for studying long-range antiferromagnetic fluctuations in the three-dimensional Hubbard model. The interplay of these nonlocal spin fluctuations with the local DMFT fluctuations is surprising: Close to the metal-insulator transition, the nonlocal fluctuations strongly suppress the spectral function, in contrast to the weak-coupling expectation for three dimensions.[18]

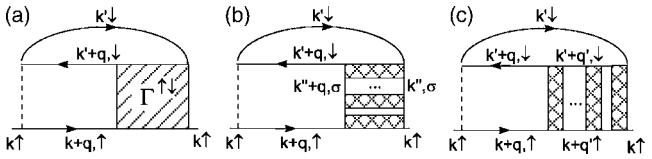

FIG. 1. (a) From the reducible vertex, we directly obtain the self-energy. (b) and (c) The two particle-hole channels contributing to the self-energy (longitudinal and transversal) in the ladder approximation. Instead of the bare interaction, ladder diagrams are constructed from the irreducible local vertices (crosshatched) in DΓA.

The plan of the paper is the following. In Sec. II, we introduce the DΓA. Specifically, we derive the full DΓA scheme based on the parquet equations in Sec. II A, and a simplified version based on a ladder subset of diagrams in Sec. II B. The latter yields the most important diagrams for the specific problem considered in this paper, i.e., the paramagnon fluctuations in the proximity of the AF transition. We compare this approach with the $1/d$ expansion in Sec. II C. The details concerning the calculation of the local vertex within an exact diagonalization impurity solver are reported in Sec. III (and in the Appendix). Results for the local irreducible vertex and the DΓA self-energy and spectral functions are presented in Secs. IV A and IV B, respectively. Finally, we give a conclusion and discuss the potential of our method in Sec. V.

II. DYNAMICAL VERTEX APPROXIMATION

The starting point of our considerations is the Hubbard model on a cubic lattice,

$$H = -t\sum_{\langle ij\rangle\sigma} c^{\dagger}_{i\sigma}c_{j\sigma} + U\sum_{i} n_{i\uparrow}n_{i\downarrow}, \tag{1}$$

where t denotes the hopping amplitude between nearest neighbors, U the Coulomb interaction, $c^{\dagger}_{i\sigma}$ ($c_{i\sigma}$) creates (annihilates) an electron with spin σ on site i, and $n_{i\sigma}=c^{\dagger}_{i\sigma}c_{i\sigma}$. In the following, we restrict ourselves to the paramagnetic phase with n electrons/site and temperature T.

Let us suppose we know the two-particle vertex $\Gamma^{\nu\nu'\omega\uparrow\downarrow}_{\mathbf{k}\mathbf{k}'\mathbf{q}}$. Then, we can calculate the (nonlocal) self-energy through the exact relation [following from the equation of motion; see Fig. 1(a) and, e.g., Refs. 20 and 21]

$$\Sigma_{\mathbf{k},\nu} = U\frac{n}{2} - T^2U\sum_{\substack{\nu'\omega\\ \mathbf{k}'\mathbf{q}}} \Gamma^{\nu\nu'\omega\uparrow\downarrow}_{\mathbf{k}\mathbf{k}'\mathbf{q}} G_{\mathbf{k}'+\mathbf{q},\nu'+\omega} G_{\mathbf{k}',\nu'} G_{\mathbf{k}+\mathbf{q},\nu+\omega}, \tag{2}$$

where $G_{\mathbf{k},\nu}=(i\nu_n-\epsilon_{\mathbf{k}}+\mu-\Sigma_{\mathbf{k},\nu})^{-1}$ is the nonlocal Green function, $\epsilon_{\mathbf{k}}=-2t\Sigma_{\alpha=x,y,z}\cos k_{\alpha}$ is the bare electronic dispersion, and μ is the electronic chemical potential. Generally, $\Gamma^{\nu\nu'\omega\uparrow\downarrow}_{\mathbf{k}\mathbf{k}'\mathbf{q}}$ can be expressed diagrammatically, e.g., by taking the fully two-, three-, and more-particle irreducible local vertices as building blocks and connecting these blocks by local and nonlocal Green functions.

A. Parquet equations

In the DΓA, we restrict ourselves to the local fully irreducible two-particle vertices $\Gamma^{\mathrm{loc}}_{\mathrm{fir}}$. From these building blocks, the reducible vertices $\Gamma^{\nu\nu'\omega\uparrow\downarrow}_{\mathbf{k}\mathbf{k}'\mathbf{q}}$ can be obtained through the self-consistent solution of the parquet equations.[19,20] Representing this vertex as a sum of contributions of different channels, one has[19–21]

$$\Gamma^{\nu\nu'\omega\uparrow\downarrow}_{\mathbf{k}\mathbf{k}'\mathbf{q}} = \Gamma^{\nu\nu'\omega,\uparrow\downarrow}_{\mathrm{fir,loc}} + C^{\nu\nu'\omega}_{\mathbf{k}\mathbf{k}'\mathbf{q}} + Z^{\nu\nu'\omega}_{\mathbf{k}\mathbf{k}'\mathbf{q}} + \tilde{Z}^{\nu\nu'\omega}_{\mathbf{k}\mathbf{k}'\mathbf{q}}, \tag{3}$$

$$\Gamma^{\nu\nu'\omega\uparrow\uparrow}_{\mathbf{k}\mathbf{k}'\mathbf{q}} = \Gamma^{\nu\nu'\omega\uparrow\downarrow}_{\mathbf{k}\mathbf{k}'\mathbf{q}} - \bar{\Gamma}^{\nu\nu'\omega\uparrow\downarrow}_{\mathbf{k}\mathbf{k}'\mathbf{q}}. \tag{4}$$

Here, $\bar{\Gamma}^{\nu\nu'\omega\uparrow\downarrow}_{\mathbf{k}\mathbf{k}'\mathbf{q}}=\Gamma^{\nu,\nu+\omega,\nu-\nu'\uparrow\downarrow}_{\mathbf{k},\mathbf{k}+\mathbf{q},\mathbf{k}-\mathbf{k}'}$ and the contribution of the three channels can be written in the following form (see Fig. 2):

$$C^{\nu\nu'\omega}_{\mathbf{k}\mathbf{k}'\mathbf{q}} = \Gamma^{\uparrow\downarrow} * G * G * (\Gamma^{\uparrow\downarrow}_{\mathrm{fir,loc}} + Z + \tilde{Z}), \tag{5}$$

$$Z^{\nu\nu'\omega}_{\mathbf{k}\mathbf{k}'\mathbf{q}} = \Gamma^{\uparrow\downarrow} * G * G * (\Gamma^{\uparrow\downarrow}_{\mathrm{fir,loc}} + C + \tilde{Z}), \tag{6}$$

$$\begin{aligned}\tilde{Z}^{\nu\nu'\omega}_{\mathbf{k}\mathbf{k}'\mathbf{q}} = {} & (\Gamma^{\uparrow\uparrow} + \Gamma^{\uparrow\downarrow}) * G * G * (\Gamma^{\uparrow\downarrow}_{\mathrm{fir,loc}} + C + Z)\\ & - \Gamma^{\uparrow\downarrow} * G * G * (\bar{\Gamma}^{\uparrow\downarrow}_{\mathrm{fir,loc}} + \bar{C} + \bar{Z}),\end{aligned} \tag{7}$$

where $*$ stands for multiplication and summation over the momenta and frequencies given in Fig. 2.

For determining the fully irreducible local vertex $\Gamma^{\mathrm{loc}}_{\mathrm{fir}}$, which is constructed from purely local Feynman diagrams only, we resort to the Anderson impurity model (AIM).[22] In fact, the AIM has only one interacting site, so it yields the same local diagrams—and hence the same irreducible vertex—provided that the local Green function is identical. Hence a practical way to obtain $\Gamma^{\mathrm{loc}}_{\mathrm{fir}}$ is through the (e.g., numerical) solution of the AIM. The starting point can be the (local) spin and charge susceptibility of the AIM,

$$\chi^{\nu\nu'\omega}_{s(c),\mathrm{loc}} = \chi^{\nu\nu'\omega,\uparrow\uparrow}_{\mathrm{loc}} \underset{(-)}{+} \chi^{\nu\nu'\omega,\uparrow\downarrow}_{\mathrm{loc}}, \tag{8}$$

from which we can obtain the full (reducible) local vertex $\Gamma_{s(c),\mathrm{loc}}$ and the irreducible local vertices in the spin-, charge-, and particle-particle channel ($\Gamma_{s,\mathrm{ir}}$, $\Gamma_{c,\mathrm{ir}}$, and $\Gamma_{pp,\mathrm{ir}}$, respectively) via the standard relations

$$\chi^{\nu\nu'\omega}_{s(c),\mathrm{loc}} = \chi^{\nu}_{0\omega,\mathrm{loc}}\delta_{\nu\nu'} + \chi^{\nu}_{0\omega,\mathrm{loc}}\Gamma^{\nu\nu'\omega}_{s(c),\mathrm{loc}}\chi^{\nu'}_{0\omega,\mathrm{loc}}, \tag{9}$$

$$\Gamma^{\nu\nu'\omega}_{s(c),\mathrm{loc}} = [(\Gamma^{\nu\nu'\omega}_{s(c),\mathrm{ir}})^{-1} - \chi^{\nu'}_{0\omega,\mathrm{loc}}\delta_{\nu\nu'}]^{-1}, \tag{10}$$

$$\Gamma^{\nu\nu'\omega,\uparrow\downarrow}_{pp,\mathrm{loc}} = [(\Gamma^{\nu,\nu',\tilde{\nu}-\nu}_{pp,\mathrm{ir}})^{-1}_{\nu,\tilde{\nu}} - \Pi^{\tilde{\nu}}_{0\tilde{\nu}+\nu',\mathrm{loc}}\delta_{\nu\tilde{\nu}}]^{-1}_{\tilde{\nu}=\nu+\omega}, \tag{11}$$

where

$$\begin{aligned}\chi^{\nu'}_{0\omega,\mathrm{loc}} &= -TG_{\mathrm{loc}}(\nu')G_{\mathrm{loc}}(\omega+\nu'),\\ \Pi^{\nu'}_{0\omega,\mathrm{loc}} &= TG_{\mathrm{loc}}(\nu')G_{\mathrm{loc}}(\omega-\nu').\end{aligned} \tag{12}$$

From these vertices, we can in turn calculate the fully irreducible vertex as

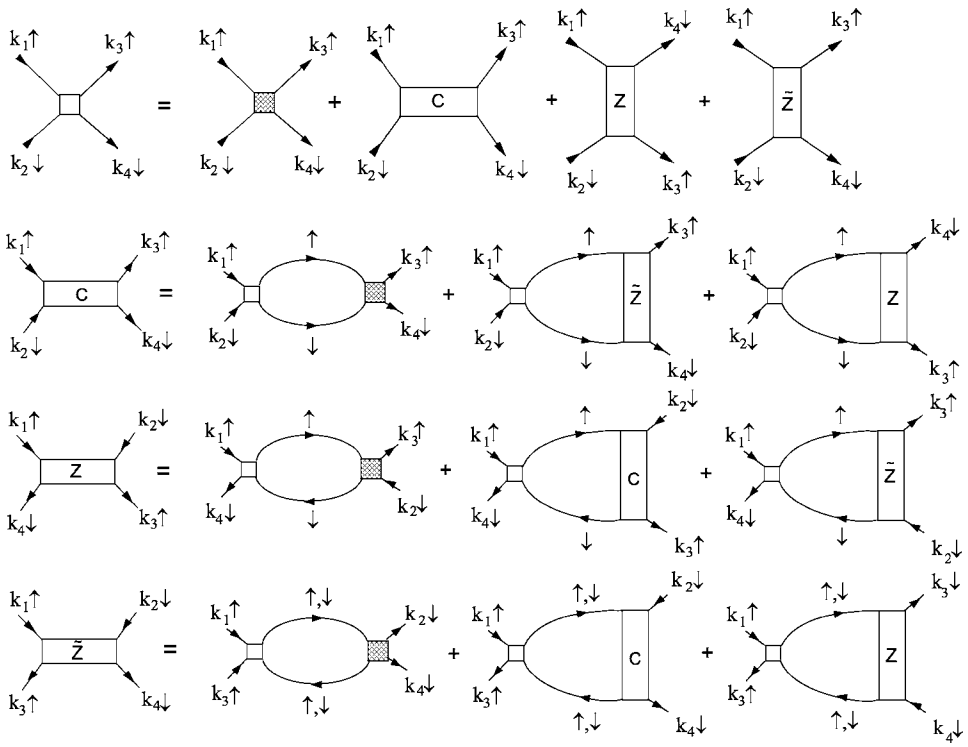

FIG. 2. Graphical notation of the parquet Eqs. (3) and (5)–(7). C, Z, and $\tilde{Z}$ denote the contributions of the particle-particle, particle-hole, and interaction channels to the nonlocal vertex $\Gamma^{\nu_1,\nu_4,\nu_3-\nu_1,\uparrow\downarrow}_{\mathbf{k}_1,k_4,k_3-k_1}$ (the momentum and frequency $\mathbf{k}_2,\nu_2$ are determined by conservation laws).

$$\Gamma^{\nu\nu'\omega,\uparrow\downarrow}_{\mathrm{fir,loc}} = \frac{1}{2}(\Gamma^{\nu\nu'\omega}_{s,\mathrm{ir}} - \Gamma^{\nu\nu'\omega}_{c,\mathrm{ir}}) + \Gamma^{\nu,\nu+\omega,\nu'-\nu}_{s,\mathrm{ir}} + \Gamma^{\nu\nu'\omega}_{pp,\mathrm{ir}} - 2\Gamma^{\nu\nu'\omega\uparrow\downarrow}_{\mathrm{loc}}. \tag{13}$$

B. Ladder approximation

In this paper, we are particularly interested in paramagnon contributions affecting the self-energy in the vicinity of the antiferromagnetic phase. Hence, as discussed in the Introduction and with some justification in $1/d$ (see Sec. II C), we restrict ourselves to the ladder subset of the parquet diagrams in the two particle-hole channels shown in Figs. 1(b) and 1(c). These diagrams can be derived from the general parquet set of diagrams of Fig. 2, supposing the locality of $C,Z,\tilde{Z}$ on the right-hand side of Eqs. (5)–(7). Expressing the ladder diagrams through the vertices in the spin (s) and charge (c) channels $\Gamma^{\nu\nu'\omega}_{s(c),\mathbf{q}}$, which depend on the momentum transferred $\mathbf{q}$ only, the sum of the vertices of Figs. 1(b) and 1(c) is obtained as

$$\Gamma^{\nu\nu'\omega,\uparrow\downarrow}_{\mathbf{k}\mathbf{k}'\mathbf{q}} = \frac{1}{2}(\Gamma^{\nu\nu'\omega}_{s,\mathbf{q}} - \Gamma^{\nu\nu'\omega}_{c,\mathbf{q}}) + \Gamma^{\nu,\nu+\omega,\nu'-\nu}_{s,\mathbf{k}'-\mathbf{k}} - \frac{1}{2}(\Gamma^{\nu\nu'\omega}_{s,\mathrm{loc}} - \Gamma^{\nu\nu'\omega}_{c,\mathrm{loc}}). \tag{14}$$

Here, the first two terms of Eq. (14) describe the longitudinal and transverse paramagnons in Figs. 1(b) and 1(c), respectively, and the last term subtracts the double-counted local contribution. Note that the nonlocal contribution of the particle-particle channel to the self-energy, which is not relevant near magnetic instabilities, has been neglected here.

The quantities on the right-hand side of Eq. (14) are calculated from the local vertex $\Gamma^{\nu\nu'\omega}_{s(c),\mathrm{ir}}$, irreducible in the spin (charge) channel, via

$$\Gamma^{\nu\nu'\omega}_{s(c),\mathbf{q}} = [(\Gamma^{\nu\nu'\omega}_{s(c),\mathrm{ir}})^{-1} - \chi^{\nu'}_{0\mathbf{q}\omega}\delta_{\nu\nu'}]^{-1}, \tag{15}$$

where $\chi^{\nu'}_{0\mathbf{q}\omega} = -T\Sigma_{\mathbf{k}} G_{\mathbf{k},\nu'} G_{\mathbf{k}+\mathbf{q},\nu'+\omega}$ with $G_{\mathbf{k},\nu} = [i\nu - \epsilon_{\mathbf{k}} + \mu - \Sigma_{\mathrm{loc}}(\nu)]^{-1}$, Σ_{loc} being the local (DMFT) self-energy. Note that contrary to the full parquet solution in Sec. II A, the self-energy of the internal Green functions is considered purely local in accordance with the assumption of the locality of the vertex $\Gamma^{\nu\nu'\omega}_{s(c),\mathrm{ir}}$. The results of this non-self-consistent approach are expected to be close to those of the self-consistent one, due to the cancellations between (self-consistent) nonlocal self-energy and corresponding corrections to the vertex $\Gamma_{s(c),\mathrm{ir}}$, cf. Ref. 23.

Substituting Eq. (14) into Eq. (2), we obtain after a shift of the momenta and frequencies

$$\Sigma_{\mathbf{k},\nu} = \frac{1}{2}Un + \frac{1}{2}TU\sum_{\nu'\omega,\mathbf{q}} \chi^{\nu'}_{0\mathbf{q}\omega}(3\Gamma^{\nu\nu'\omega}_{s,\mathbf{q}} - \Gamma^{\nu\nu'\omega}_{c,\mathbf{q}} + \Gamma^{\nu\nu'\omega}_{c,\mathrm{loc}} - \Gamma^{\nu\nu'\omega}_{s,\mathrm{loc}})G_{\mathbf{k}+\mathbf{q},\nu+\omega}. \tag{16}$$

Equation (16) reduces to the DMFT self-energy if the nonlocal quantities are replaced by local ones. But beyond that, it describes the nonlocal ladder diagrams of Figs. 1(b) and 1(c).

C. Comparison to the $1/d$ expansion

Let us compare the result Eq. (16) to that of the $1/d$ expansion. While the DMFT self-energy contains the local

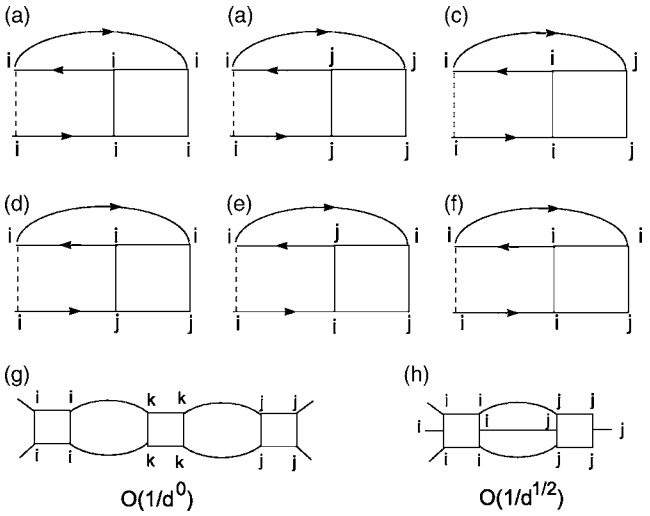

FIG. 3. Diagrams for the self-energy in terms of the vertex to order $1/d^0$ [(a), i.e., DMFT] and $1/d^{1/2}$ [(b)–(f)]. The ladder diagram (g) shows how diagrams (b)–(e) can be constructed from a fully irreducible local two-particle vertex. In contrast, for diagram (f) a local three-particle vertex is needed, see (h). Hence the contribution (f) is the only one not included in the DΓA.

Green functions and vertex only [Fig. 3(a)], the leading nonlocal corrections to the self-energy are proportional to $O(1/d^{1/2})$ and the consideration of the diagrams containing two different sites is sufficient at this order.[4] The possible types of these diagrams for the self-energy are shown in Figs. 3(b)–3(f). The first type of corrections [Fig. 3(b)] involves the nonlocal Green functions only. The second type of corrections [Figs. 3(c)–3(e)] contains the nonlocal vertices with two legs at i and two at j sites. To leading (zeroth) order in $1/d$, these vertices can be expressed as a ladder of local vertices connected by the nonlocal Green functions, as in Fig. 3(g). The contributions of Figs. 3(b)–3(e) are hence included in the DΓA with the ladder approximation, i.e., in Eq. (16). The last type of $1/d^{1/2}$ corrections to the self-energy [Fig. 3(f)] involves the three-particle local vertex [Fig. 3(h)] [and are of order $(U/t)^5$]. According to the classification of the Introduction, these corrections should be taken into account on the next level of approximation beyond DΓA and are the only $1/d^{1/2}$ corrections neglected in DΓA. Therefore, the DΓA reproduces correctly the leading $1/d$ correction to the self-energy with the three-particle local vertex neglected.

III. CALCULATION OF THE LOCAL FOUR-POINT VERTEX

The calculation of the self-energy (16) requires the knowledge of the local vertex, either fully irreducible—for the general scheme—or irreducible in the spin (charge) channel—for the ladder diagrams of Figs. 1(b) and 1(c) [Eq. (16)]. As already noted, this local vertex can be obtained numerically from the Anderson impurity model. For obtaining the four-point vertex $\Gamma^{\nu'\nu\omega}_{s(c),\mathrm{loc}}$, we need to calculate the AIM susceptibility for three Matsubara frequencies,[24]

$$\chi^{\nu\nu'\omega\sigma\sigma'}_{\mathrm{loc}} = T^2 \int_0^{1/T} d\tau_1 d\tau_2 d\tau_3 e^{-i\tau_1\nu} e^{i\tau_2(\nu+\omega)} e^{-i\tau_3(\nu'+\omega)} \times [\langle T_\tau c^\dagger_{i\sigma}(\tau_1) c_{i\sigma}(\tau_2) c^\dagger_{i\sigma'}(\tau_3) c_{i\sigma'}(0)\rangle - \langle T_\tau c^\dagger_{i\sigma}(\tau_1) c_{i\sigma}(\tau_2)\rangle \langle T_\tau c^\dagger_{i\sigma'}(\tau_3) c_{i\sigma'}(0)\rangle], \tag{17}$$

where ν, ν' and ω are the two fermionic and the bosonic (transferred) Matsubara frequency, respectively; $\langle T_\tau \cdots \rangle$ indicates the thermal expectation value of the time-ordered operators and the last term represents the nonconnected contributions. With a spin (anti)symmetrization (8), we obtain the corresponding charge and spin susceptibilities $\chi^{\nu\nu'\omega}_{s(c),\mathrm{loc}}$. From these, we can either determine the fully irreducible local vertex and through the parquet equations the reducible vertex and the self-energy along the lines of Eqs. (13), (3), and (2), or we can directly calculate the particle-hole ladders along the lines of Eqs. (14) and (16). We implement the latter by (i) solving the DMFT equations using exact diagonalization (ED), (ii) calculating via Eq. (17) the local vertices, and (iii) constructing from these through Eq. (16) the DΓA self-energy. In principle, this k-dependent self-energy yields new Green functions and a new vertex. However, because of the ladder approximation, we do not perform such a self-consistent calculation here.

Within ED, the calculation of χ_{loc} [Eq. (17)] is straightforwardly (albeit lengthy) performed by resorting to its Lehmann representation, whose explicit expression is reported in the Appendix. The Lehmann representation of χ_{loc} requires four summations over all the Hilbert states of the discretized AIM (compared with only two summations for evaluating the local Green function). This is the higher computational cost of DΓA compared with DMFT. By performing a parallel computation of χ_{loc}, we were able to calculate AIMs with $N_s=5$ sites and evaluate χ_{loc} for the lowest $N_{\mathrm{max}}=20$ (or, in some cases, 25) Matsubara frequencies. This turned out to be sufficient for getting a stable analytic continuation of Eq. (16), using the Padé algorithm. For the momentum summation of Eq. (16), we have used $N_k=96$ points for each directions.

IV. RESULTS

A. Local vertex close to a Mott-Hubbard transition

First, we discuss our results for the local irreducible vertex. Since we are mainly interested in long-range antiferromagnetic fluctuations, we consider temperatures slightly above the DMFT Néel temperature (see the inset of Fig. 4). In this case, the largest contribution to the nonlocal part of the DΓA self-energy stems from the terms of Eq. (16) proportional to the local vertex irreducible in the spin channel, particularly with zero bosonic frequency.

In Fig. 4, we show the $\Gamma^{\nu\nu',\omega=0}_{s,\mathrm{ir}}$ as a function of ν' (with ν fixed to its lowest value πT) at half-filling for three different values of the Hubbard interaction ($U=1D$, $1.5D$, and $2D$, where $D=2\sqrt{6}t$ is twice the variance of the noninteracting density of states) and temperature ($T=0.067D$, $0.089D$, and

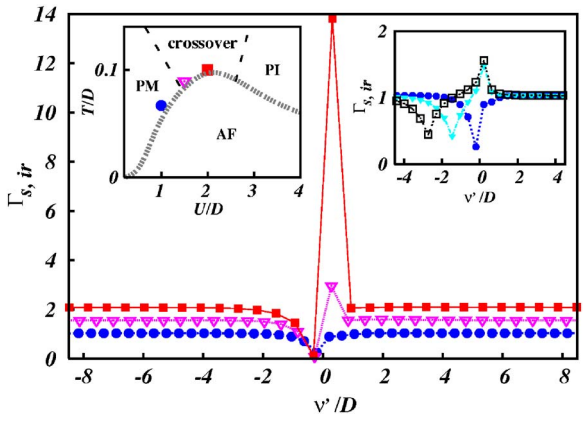

FIG. 4. (Color online) Dependence of the local vertex $\Gamma_{s,\mathrm{ir}}^{\nu=\pi T,\nu',\omega=0}$ on the incoming fermionic frequency ν', for the three different values of U and T indicated as symbols in the left inset, which shows the DMFT phase diagram with paramagnetic metallic (PM), insulating (PI), and antiferromagnetic (AF) phase. Right inset: Same as the main panel but at fixed $U=1D$ and at different ω's (circles: $\omega=0$; triangles: $\omega=6\pi T$; squares: $\omega=12\pi T$).

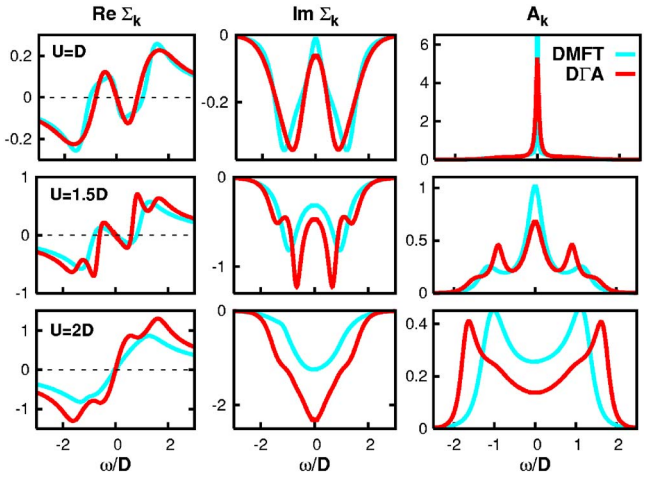

FIG. 5. (Color online) Self-energy (left: real, middle: imaginary part) and spectral function (right) at $\mathbf{k}=(\pi/2,\pi/2,\pi/2)$, $U=1D$ (top), $1.5D$ (central), and $2D$ (bottom) and the same T's of Fig. 4. Compared to DMFT (light blue line), quasiparticles are damped through scattering at nonlocal spin fluctuations in DΓA (dark red line), and the system is more insulating. At $U=1.5D$ and $2D$, these effects are drastically enhanced because of strong local correlations reflected in $\Gamma_{s,\mathrm{ir}}$

$0.1D$). This choice allows us to highlight the remarkable differences occurring when moving from the metallic regime to the crossover region of the DMFT phase diagram of the Hubbard model. In particular, we note that $\Gamma_{s,\mathrm{ir}}$ correctly approaches the corresponding value of the bare interaction U for large ν'. On the other hand, at small ν' we observe a radically different behavior of the local vertex depending on the U value: At $U=1D$, $\Gamma_{s,\mathrm{ir}}$ displays a smooth minimum in the region of small ν', while at $U=1.5D$ (and even more at $U=2D$), a very pronounced maximum of $\Gamma_{s,\mathrm{ir}}$ appears at $\nu'=\nu$. While the behavior of $\Gamma_{s,\mathrm{ir}}$ at small U can be easily interpreted as the screening of the bare interaction, typical of the metallic phase, the huge maximum of $\Gamma_{s,\mathrm{ir}}$ at larger U stems from particle-hole fluctuations in the vicinity of the metal-insulator transition, as discussed in Ref. 21.

B. DΓA self-energy and spectral function

The striking behavior of $\Gamma_{s,\mathrm{ir}}$ has consequences for the DΓA self-energy on the real axis and spectral function, presented in Fig. 5 for the same three different U's and T's of Fig. 4 (left inset).

At $U=1D$, i.e., in the metallic regime of the phase diagram, DMFT shows a quasiparticle peak that is only weakly damped for $\mathbf{k}$ vectors on the Fermi surface. In DΓA, the quasiparticle scatters at nonlocal antiferromagnetic fluctuations, resulting in a broadening of the quasiparticle with a now significant damping given by $\mathrm{Im}\,\Sigma_{\mathbf{k}}(0)$. For this U value, the distinct features of $\Gamma_{s,\mathrm{ir}}$ are not yet particularly pronounced in Fig. 4. It is the strongly enhanced antiferromagnetic susceptibility close to the Néel temperature that leads to this damping in Eq. (16). Stronger damping effects can be observed, studying the Hubbard model in $d=2$, e.g., by means of the cluster extensions of DMFT,[5] which predict a pseudogap opening at low temperatures. Actually, a stronger damping in $d=2$ than in the three-dimensional case considered here is expected from weak-coupling perturbation theory. Unfortunately, to our knowledge, no cluster-DMFT calculation has been performed for the case of $d=3$, since it poses severe constraints on the cluster size.

At $U=2D$, the stronger electronic correlation reflects in more pronounced changes of the spectral function. Now, it is the huge $\Gamma_{s,\mathrm{ir}}$ of Fig. 4 that strongly suppresses the spectral weight at the Fermi level. This weight is transferred to the Hubbard subbands, which get some additional structure as an effect of magnetic fluctuations. The nonlocal fluctuations result in a much more insulating solution, even though the Green function is still nonlocal.[25]

We emphasize that the mechanism of spectral weight suppression at $U=2D$ is very different from that in the weak-coupling regime (Ref. 18 and our $U=1D$ results), where long-range magnetic fluctuations in the immediate vicinity of the magnetic phase transition play the key role. In contrast at $U=2D$, already relatively short-range spin fluctuations are important because of the strong correlations reflected in the enhanced $\Gamma_{s,\mathrm{ir}}$. The spectral weight suppression is therefore also quite robust upon increasing T, i.e., upon going farther away from the antiferromagnetic transition (not shown).

At $U=1.5D$, we have something in between the two cases discussed above: The vertex is already enhanced, but long-range antiferromagnetic fluctuations are still essential. This leads to a suppression of the quasiparticle weight and structured Hubbard bands. Altogether this shows that scattering at nonlocal fluctuations close to a strongly correlated antiferromagnet is very different from that in the vicinity of a weakly correlated Slater antiferromagnet.

V. CONCLUSIONS

We developed the dynamical vertex approximation (DΓA) based on the assumption of the locality of the irre-

ducible vertex. For the half-filled three-dimensional Hubbard model, we found that the local vertex (irreducible in the particle-hole spin channel) strongly depends on all three frequencies; it is hugely enhanced at some particular frequencies for large U. These strong local correlations entail similarly strong nonlocal fluctuations. The scattering of the quasiparticles at these nonlocal spin fluctuations, in turn, drastically reduces their lifetimes; spectral weight is transferred to the Hubbard bands, which develop some additional structure. These nonlocal effects of strong electronic correlations are very different from those at weak coupling. It is a strength of DΓA to reveal them.

Including long-range correlations, DΓA opens the door to study a wide variety of physical phenomena, previously described only for weakly correlated systems, such as magnons in strongly correlated (anti)ferromagnets,[28] the interplay of weak localization effects and strong electron interactions, and vertex corrections to the RPA screening. A self-consistent realization of the approach might also allow us to study how nonlocal fluctuations suppress magnetic long-range ordering, whether antiferromagnetic fluctuations in the vicinity of the metal-insulator transition result in unconventional superconductivity, and how physical quantities change in the vicinity of ferro- and antiferromagnetic quantum critical points.

Note added. During the completion of our paper, we learned about a related study, Ref. 26. Also note the preprint Ref. 27.

ACKNOWLEDGMENTS

We thank W. Metzner, M. Capone, C. Castellani, G. Sangiovanni, and R. Arita for stimulating discussions; we are indebted to M. Capone also for providing the DMFT(ED) code, which served as a starting point. This work was supported by the Deutsche Forschungsgemeinschaft through the Emmy-Noether program (A.T., K.H.) and 436 RUS 113/723/0-2 (A.K.) and by the Russian Basic Research Foundation through Grant No. 747.2003.2 (A.K.).

APPENDIX: LEHMANN REPRESENTATION OF THE LOCAL SUSCEPTIBILITY

In this appendix, we report the explicit expression of the Lehmann representation for the local (and spin-dependent) susceptibility, which is necessary for performing the calculation of the basic "brick" of the DΓA (i.e., the local four-point vertex) within the ED algorithm (see Sec. III).

We start with the evaluation of the T-ordered product appearing in the definition of the (spin-dependent) local susceptibility in Eq. (17),

$$\begin{aligned}\tilde{\chi}_{\mathrm{loc}}^{\nu\nu'\omega\sigma\sigma'} &= T^2\int_0^\beta d\tau_1 d\tau_2 d\tau_3 e^{-i\tau_1\nu}e^{+i\tau_2(\nu+\omega)}e^{-i\tau_3(\nu'+\omega)}\\ &\quad\times\langle T_\tau c_{i\sigma}^\dagger(\tau_1)c_{i\sigma}(\tau_2)c_{i\sigma'}^\dagger(\tau_3)c_{i\sigma'}(0)\rangle\\ &= T^2\int_0^\beta d\tau_1\left[\int_0^{\tau_1}d\tau_2\left(\int_0^{\tau_2}d\tau_3-\int_{\tau_2}^{\tau_1}d\tau_3+\int_{\tau_1}^{\beta}d\tau_3\right)\right.\\ &\quad\left.-\int_{\tau_1}^{\beta}d\tau_2\left(\int_0^{\tau_1}d\tau_3-\int_{\tau_1}^{\tau_2}d\tau_3+\int_{\tau_2}^{\beta}d\tau_3\right)\right]\\ &\quad\times e^{-i\nu(\tau_1-\tau_2)}e^{i\omega(\tau_2-\tau_3)}e^{-i\nu'\tau_3}\langle\cdots\rangle\\ &= \frac{T^2}{Z}(\chi_{\mathrm{loc}}^{123}+\chi_{\mathrm{loc}}^{132}+\chi_{\mathrm{loc}}^{312}+\chi_{\mathrm{loc}}^{213}+\chi_{\mathrm{loc}}^{231}+\chi_{\mathrm{loc}}^{321}),\end{aligned}\tag{A1}$$

where $\beta=1/T$, Z is the partition function and with $\langle\cdots\rangle$ we indicate the thermal and quantum average of the four fermionic operators on the right-hand side of the first line of the equation, which are already ordered in terms of decreasing times (with no further sign change). The six different contributions $\chi_{\mathrm{loc}}^{123},\chi_{\mathrm{loc}}^{132},\cdots$ appearing in the last line of Eq. (A1) reflect the six different ways of arranging the order of the three Matsubara times τ_1, τ_2, and τ_3 in the time integral of Eq. (17). $\chi_{\mathrm{loc}}^{123},\chi_{\mathrm{loc}}^{132},\cdots$ can be explicitly expressed in a very convenient way for ED scheme, i.e., in terms of the eigenenergies E_N and the matrix elements $\langle N|c_\sigma^{(\dagger)}|M\rangle=(c_\sigma^{(\dagger)})_{NM}$, of the associated AIM, through the standard Lehmann representation. The evaluation of the six time integrals in Eq. (A1) is straightforward, albeit lengthy, and yields the following results:

$$\begin{aligned}\chi_{\mathrm{loc}}^{123} &= \sum_{N,M,L,S}\frac{-1}{i(\nu'+\omega)-E_L+E_S}\left[\frac{1}{i(\nu-\nu')+E_M-E_S}\left(\frac{e^{-\beta E_N}+e^{-\beta E_S}}{i\nu'-E_N+E_S}-\frac{e^{-\beta E_M}+e^{-\beta E_N}}{i\nu-E_N+E_M}\right)\right.\\ &\quad\left.-\frac{1}{i(\nu+\omega)+E_M-E_L}\left(\frac{e^{-\beta E_L}-e^{-\beta E_N}}{i\omega+E_N-E_L}-\frac{e^{-\beta E_M}+e^{-\beta E_N}}{i\nu-E_N+E_M}\right)\right](c_\sigma^\dagger)_{NM}(c_\sigma)_{ML}(c_{\sigma'}^\dagger)_{LS}(c_{\sigma'})_{SN},\end{aligned}\tag{A2}$$

$$\begin{aligned}\chi_{\mathrm{loc}}^{132} &= \sum_{N,M,L,S}\frac{1}{i(\nu'+\omega)-E_M+E_L}\left[\frac{1}{i(\nu+\omega)+E_L-E_S}\left(\frac{e^{-\beta E_N}+e^{-\beta E_S}}{i\nu'-E_N+E_S}+\frac{e^{-\beta E_L}-e^{-\beta E_N}}{i(\nu+\nu'+\omega)-E_N+E_L}\right)\right.\\ &\quad\left.+\frac{1}{i(\nu-\nu')+E_M-E_S}\left(\frac{e^{-\beta E_M}+e^{-\beta E_N}}{i\nu+E_M-E_N}-\frac{e^{-\beta E_S}+e^{-\beta E_N}}{i\nu'+E_S-E_N}\right)\right](c_\sigma^\dagger)_{NM}(c_{\sigma'}^\dagger)_{ML}(c_\sigma)_{LS}(c_{\sigma'})_{SN},\end{aligned}\tag{A3}$$

$$\chi_{\mathrm{loc}}^{213}=\sum_{N,M,L,S}\frac{1}{i(\nu'+\omega)+E_L-E_M}\frac{1}{i(\nu+\omega)+E_S-E_N}\left(\frac{e^{-\beta E_M}-e^{-\beta E_S}}{i\omega+E_S-E_M}+\frac{e^{-\beta E_L}-e^{-\beta E_N}}{i(\nu+\nu'+\omega)-E_N+E_L}+\frac{e^{-\beta E_M}+e^{-\beta E_N}}{i\nu+E_M-E_N}-\frac{e^{-\beta E_S}+e^{-\beta E_L}}{i\nu'+E_L-E_S}\right)$$
$$\times(c_\sigma^\dagger)_{NM}(c_{\sigma'}^\dagger)_{ML}(c_{\sigma'})_{LS}(c_\sigma)_{SN}, \tag{A4}$$

$$\chi_{\mathrm{loc}}^{231}=\sum_{N,M,L,S}\frac{-1}{i(\nu'+\omega)+E_M-E_N}\left[\frac{1}{i(\nu-\nu')-E_M+E_S}\left(\frac{e^{-\beta E_M}+e^{-\beta E_L}}{i\nu+E_L-E_M}-\frac{e^{-\beta E_L}+e^{-\beta E_S}}{i\nu'+E_L-E_S}\right)\right.$$
$$\left.-\frac{1}{i(\nu+\omega)+E_S-E_N}\left(\frac{e^{-\beta E_L}-e^{-\beta E_N}}{i(\nu+\nu'+\omega)+E_L-E_N}-\frac{e^{-\beta E_L}+e^{-\beta E_S}}{i\nu'+E_L-E_S}\right)\right](c_{\sigma'}^\dagger)_{NM}(c_\sigma^\dagger)_{ML}(c_{\sigma'})_{LS}(c_\sigma)_{SN}, \tag{A5}$$

$$\chi_{\mathrm{loc}}^{312}=\sum_{N,M,L,S}\frac{-1}{i(\nu'+\omega)+E_M-E_N}\frac{1}{i(\nu+\omega)+E_L-E_S}\left(\frac{e^{-\beta E_M}-e^{-\beta E_S}}{i\omega+E_M-E_S}+\frac{e^{-\beta E_L}+e^{-\beta E_M}}{i\nu+E_L-E_M}-\frac{e^{-\beta E_N}+e^{-\beta E_S}}{i\nu'+E_S-E_N}+\frac{e^{-\beta E_N}-e^{-\beta E_L}}{i(\nu+\nu'+\omega)+E_L-E_N}\right)$$
$$\times(c_{\sigma'}^\dagger)_{NM}(c_\sigma^\dagger)_{ML}(c_\sigma)_{LS}(c_{\sigma'})_{SN}, \tag{A6}$$

$$\chi_{\mathrm{loc}}^{321}=\sum_{N,M,L,S}\frac{1}{i(\nu'+\omega)+E_M-E_N}\left[\frac{1}{i(\nu+\omega)+E_M-E_L}\left(\frac{e^{-\beta E_S}+e^{-\beta E_L}}{i\nu+E_S-E_L}+\frac{e^{-\beta E_S}-e^{-\beta E_M}}{i\omega+E_M-E_S}\right)\right.$$
$$\left.-\frac{1}{i(\nu-\nu')+E_N-E_L}\left(\frac{e^{-\beta E_S}+e^{-\beta E_L}}{i\nu+E_S-E_L}-\frac{e^{-\beta E_S}+e^{-\beta E_N}}{i\nu'+E_S-E_N}\right)\right](c_{\sigma'}^\dagger)_{NM}(c_\sigma)_{ML}(c_\sigma^\dagger)_{LS}(c_{\sigma'})_{SN}. \tag{A7}$$

After the DMFT self-consistency condition has been fulfilled, the ED-DMFT evaluation of the local susceptibility Eq. (17) is obtained directly by plugging the eigenvalues E_N and the matrix elements $(c_\sigma)_{NM}$ of the associated AIM in Eqs. (A2)–(A7) and performing the corresponding four summations over the Hilbert space. The relevant numerical effort related to the Hilbert space summations can be handled by means of a parallel computations for the case considered here (i.e., $N_s=5$ and $N_{\max}\geqslant 20$), states for which all Boltzmann weights ($e^{-\beta E}$) or matrix elements that are smaller than 10^{-6} are neglected.

For the numerical implementation, let us note that some denominators in Eqs. (A2)–(A7), characterized by a bosonic Matsubara frequency [e.g., those with $i\omega$ or with $i(\nu-\nu')$], can vanish during the summations over the Hilbert space.

However there are no divergences, since the corresponding numerators are simultaneously vanishing, so that their limit is always well defined. To avoid computational problems, we simply add a very small energy shift in all the terms with a vanishing denominator (e.g., $E_N\rightarrow E_N+10^{-8}$), in order to evaluate numerically the correct limiting values.

[1] N. F. Mott, Rev. Mod. Phys. **40**, 677 (1968); *Metal-Insulator Transitions* (Taylor & Francis, London, 1990); F. Gebhard, *The Mott Metal-Insulator Transition* (Springer, Berlin, 1997).

[2] W. Metzner and D. Vollhardt, Phys. Rev. Lett. **62**, 324 (1989);

[3] A. Georges, G. Kotliar, W. Krauth, and M. Rozenberg, Rev. Mod. Phys. **68**, 13 (1996); G. Kotliar and D. Vollhardt, Phys. Today **57**(3), 53 (2004).

[4] A. Schiller and K. Ingersent, Phys. Rev. Lett. **75**, 113 (1995).

[5] M. H. Hettler, A. N. Tahvildar-Zadeh, M. Jarrell, T. Pruschke, and H. R. Krishnamurthy, Phys. Rev. B **58**, R7475 (1998); C. Huscroft, M. Jarrell, Th. Maier, S. Moukouri, and A. N. Tahvildarzadeh, Phys. Rev. Lett. **86**, 139 (2001); A. I. Lichtenstein and M. I. Katsnelson, Phys. Rev. B **62**, R9283 (2000); G. Kotliar, S. Y. Savrasov, G. Pàlsson, and G. Biroli, Phys. Rev. Lett. **87**, 186401 (2001); T. A. Maier, M. Jarrell, T. Pruschke, M. H. Hettler, Rev. Mod. Phys. **77**, 1027 (2005).

[6] Cluster sizes can be extended by using, e.g., the fluctuation exchange approximation, see K. Aryanpour, M. H. Hettler, and M. Jarrell, Phys. Rev. B **67**, 085101 (2003).

[7] N. E. Bickers, D. J. Scalapino, and S. R. White, Phys. Rev. Lett. **62**, 961 (1989).

[8] Y. M. Vilk and A. M. S. Tremblay, J. Phys. I **7**, 1309 (1997).

[9] D. Zanchi and H. J. Schulz, Phys. Rev. B **54**, 9509 (1996); C. J. Halboth and W. Metzner, Phys. Rev. Lett. **85**, 5162 (2000); C. Honerkamp, M. Salmhofer, N. Furukawa, and T. M. Rice, Phys. Rev. B **63**, 035109 (2001); C. Honerkamp and M. Salmhofer, Phys. Rev. Lett. **87**, 187004 (2001); A. A. Katanin and A. P. Kampf, Phys. Rev. B **68**, 195101 (2003).

[10] V. G. Vaks, A. I. Larkin, and S. A. Pikin, Zh. Eksp. Teor. Fiz. **53**, 281 (1967); [Sov. Phys. JETP **26**, 188 (1968)]; **53**, 1089 (1967); [**26**, 647 (1968)].

[11] T. Moriya, *Spin Fluctuations in Itinerant Electron Magnetism* (Springer, Berlin, 1985).

[12] A. Georges and J. S. Yedidia, Phys. Rev. B **43**, 3475 (1991), P. G.

J. van Dongen, *ibid.* **50**, 14016 (1994).
[13] V. Janiš, Phys. Rev. B **64**, 115115 (2001).
[14] E. Z. Kuchinskii, I. A. Nekrasov, and M. V. Sadovskii, JETP Lett. **82**, 198 (2005); M. V. Sadovskii, I. A. Nekrasov, E. Z. Kuchinskii, Th. Pruschke, and V. I. Anisimov, Phys. Rev. B **72**, 155105 (2005).
[15] T. Saso, J. Phys. Soc. Jpn. **68**, 3941 (1999).
[16] S. Biermann, F. Aryasetiawan, and A. Georges, Phys. Rev. Lett. **90**, 086402 (2003).
[17] Q. Si and J. L. Smith, Phys. Rev. Lett. **77**, 3391 (1996); H. Kajueter, Ph.D. thesis, Rutgers University, (1996).
[18] J. M. Vilk and A.-M. S. Tremblay J. Phys. I **7**, 1909 (1997).
[19] Y. A. Bychkov, L. P. Gor'kov, and I. E. Dzyaloshinskii, Zh. Eksp. Teor. Fiz. **50**, 738 (1966) [Sov. Phys. JETP **23**, 489 (1966)].
[20] N. E. Bickers and S. R. White, Phys. Rev. B **43**, 8044 (1991).
[21] V. Janiš, Phys. Rev. B **60**, 11345 (1999).
[22] For the physics of the AIM, see, e. g., P. W. Anderson, in *Moment Formation in Solids*, edited by W. J. L. Buyers (Plenum Press, New York, 1984); A. C. Hewson, *The Kondo Problem to Heavy Fermions*, Cambridge Studies in Magnetism Vol. 2 (Cambridge University Press, Cambridge, 1993).
[23] W. Metzner, C. Castellani, and C. Di Castro, Adv. Phys. **47**, 317 (1998).
[24] This three-frequency vertex was already introduced in Ref. 3, but, to our knowledge, only the static ($\omega=0$) vertex has been calculated, and used for computing DMFT static susceptibilities.
[25] Let us note that the analytical continuation sometimes also shows a little bump for the $U=2D$ case. But quantitatively the results are very similar.
[26] H. Kusunose, J. Phys. Soc. Jpn. **75**, 054713 (2006).
[27] C. Slezak, M. Jarrell, Th. Maier, and J. Deisz, cond-mat/0603421 (unpublished).
[28] The generalization of the DΓA to the case of magnetically ordered phases is straightforward, albeit lengthy: it is necessary to consider different vertices for the longitudinal and transverse spin fluctuations.